RESEARCH ARTICLE

Density field of supersonic separated flow past an afterbody nozzle using tomographic reconstruction of BOS data

L. Venkatakrishnan · P. Suriyanarayanan

Abstract The background oriented Schlieren (BOS) technique has been applied to determine the density field in an oblique shock-separated turbulent boundary flow. Measurements were made for two cases, namely, with/without jet flow from the afterbody which is a nozzle. In addition, oil flow and Schlieren visualizations were carried out—the results show certain upstream features of interest including shock excursions. The mean density field from BOS is discussed along with results from conventional Schlieren flow visualization. The data extracted from the mean density field obtained through BOS have been compared for the jet-off and jet-on cases. The data obtained also show the mean density in the base region (jet-off case) to be about 50% of the freestream density and match the isentropic values for the underexpanded jet at the exit. The study involving shock–boundary interaction, movement of freestream shock over the afterbody in the presence of a jet plume provides understanding of flow physics in a flow regime where whole field velocity measurements are extremely difficult.

List of symbols

M_∞ oncoming freestream Mach number (= 1.34)
P_{oj} jet total pressure
P_e jet exit pressure
P_∞ freestream static pressure at M_∞
ρ_∞ freestream static density at M_∞
D_m afterbody diameter (= 127 mm)
D nozzle exit diameter (= 63.5 mm)
δ_o boundary layer thickness on the model (= 8 mm)
L afterbody length (= 163 mm)
JPR jet pressure ratio (P_{oj}/P_∞)
X streamwise coordinate
Y, z axes perpendicular to flow direction

L. Venkatakrishnan (✉) · P. Suriyanarayanan
Experimental Aerodynamics Division,
National Aerospace Laboratories,
Council of Scientific and Industrial Research,
Bangalore, India
e-mail: venkat@ead.cmmacs.ernet.in

1 Introduction

Flow interactions taking place near the aft end of a flight vehicle can have significant effects on performance. In the presence of a jet plume, the velocity gradients existing between the jet and external flow determine the drag characteristics of the afterbody. At transonic speeds the afterbody/nozzle drag can be as large as 20% of total drag for a typical fighter aircraft or up to 70% of total drag for a missile (Midgal et al. 1969; Delery and Sirieix 1979). Several investigations (Bergman 1971; Mathur and Yajnik 1990) have been reported in literature and Schlieren studies carried out (Mathur and Yajnik 1990) to improve understanding of the behavior of such flows, particularly shocks and their movements and shock–boundary layer interaction over the afterbody in the presence of a jet. However, experimental data related to the confluence of the external supersonic flow and the jet are relatively scarce. The flow past a jet-on afterbody has been the subject of several investigations (Depres et al. 2004). Measurements carried out include mean velocity profiles, wall pressure measurements both static pressure and unsteady measurements (Reijasse et al. 1997), by usage of pressure-sensitive paints (Boswell and Dutton 2001) or flow field measurements

using LDV (Reijasse et al. 1997) and visualizations using Schlieren (Reijasse et al. 1997), Mie Scattering (Boswell and Dutton 2001). Flow field measurements are difficult in high-speed flows in general and separated flows in particular. Measurement of the mean density field in separated flows not only enhances our broad understanding of these flows, but also provides valuable data for CFD code development and validation.

There have been several efforts at quantifying the density gradient field using either the "synthetic Schlieren" method (Dalziel et al. 2000; Sutherland et al. 1999) or the "Background Oriented Schlieren"—BOS (Meier 2002; Raffel et al. 2000). The synthetic Schlieren has been successfully used for measuring amplitudes of waves generated by an oscillating cylinder (Sutherland et al. 1999; Dalziel et al. 2000; Sutherland and Linden 2002) and by an oscillating sphere (Onu et al. 2003) in a stratified flow. Venkatakrishnan and Meier (2004) validated the background oriented Schlieren (BOS) technique combined with filtered back-projection tomography, which provides the mean density field in a 2D plane. The extraction of a desired plane using filtered back-projection tomography was carried out by Venkatakrishnan (2005), who mapped the center plane of both a 4-jet cruciform configuration and a highly underexpanded supersonic axisymmetric jet. Recently, Goldhahn and Seume (2007) have assessed the accuracy, resolution, and sensitivity of the BOS system and applied it to obtain the density field of an underexpanded jet. Decamp et al. (2008) have carried out 3D synthetic Schlieren measurements using inverse tomography on idealized buoyancy fields. However, their study is limited to determination of vertical displacements as the imaged background consisted of horizontal lines rather than dots.

This paper is an attempt to document the 3D mean density field by reconstruction of the data from BOS in a supersonic shock-separated flow at the aft end of an axisymmetric body including jet effects. Density measurements were made for the free base (i.e., afterbody nozzle without the central jet) and also with an underexpanded sonic jet run at a JPR (Jet Pressure Ratio) of 6. Measurements also included surface pressure measurements on the afterbody and flow visualization with spark Schlieren and surface flow with oil flow visualization. The complex nature of the flow interactions is discussed based on the density field measurements.

2 Background oriented Schlieren methodology

The principle of the technique is the refractive index variation due to density gradients in the flow (Fig. 1). The determination of the density field using BOS thus involves the following steps: (a) calculation of displacements in the
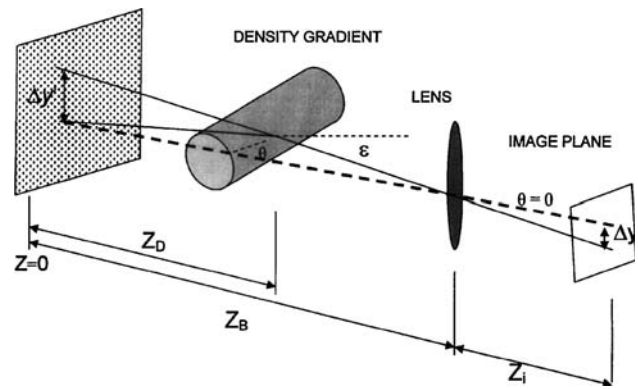

Fig. 1 Optical path for density gradient measurements by light deflection (from Venkatakrishnan and Meier 2004)

background which is imaged through the flow of interest. This is done through a (in-house) PIV-type cross-correlation algorithm. These displacements are the vectors of density gradient at each point; (b) calculation of the line-of-sight integrated density field by solution of the Poisson equation, which is the gradient of the above displacement; (c) use of optical tomography (filtered back-projection) to determine the density field in the actual plane of interest. The reader is referred to Venkatakrishnan and Meier (2004) for a derivation of the reconstruction function. The reconstruction of the entire field is achieved by inverse tomography.

3 Experimental setup and procedure

3.1 Facility and afterbody model

The experiments were carried out in the 0.5 m base flow facility wind tunnel at the National Aerospace Laboratories (Fig. 2a). This facility has a moving (variable geometry axisymmetric) outer nozzle around a center body which has the provision to provide a supersonic jet flow or multiple jets of desired Mach number. The position of the outer body of the nozzle can be set to generate different axisymmetric supersonic Mach number flows up to 3.5 around the center body. The facility provides for testing at relatively high Reynolds numbers of 10–50 million m^{-1} which corresponds to $Re \sim$ 1.3–6.4 million based on the model (center body) diameter of 127 mm. This results in a turbulent boundary layer on the afterbody ahead of the metric/non-metric split whose properties have been documented over the Mach number range of operation.

For the current freestream Mach number of 1.34, this results in a boundary layer thickness (δ_b) of 8 mm (For details see Mathur and Viswanath 2004). In the present study, the afterbody was a boat-tailed configuration of circular-arc geometry (similar to that used in several

Fig. 2 a Schematic of base flow facility (top view). **b** Detail of afterbody nozzle model
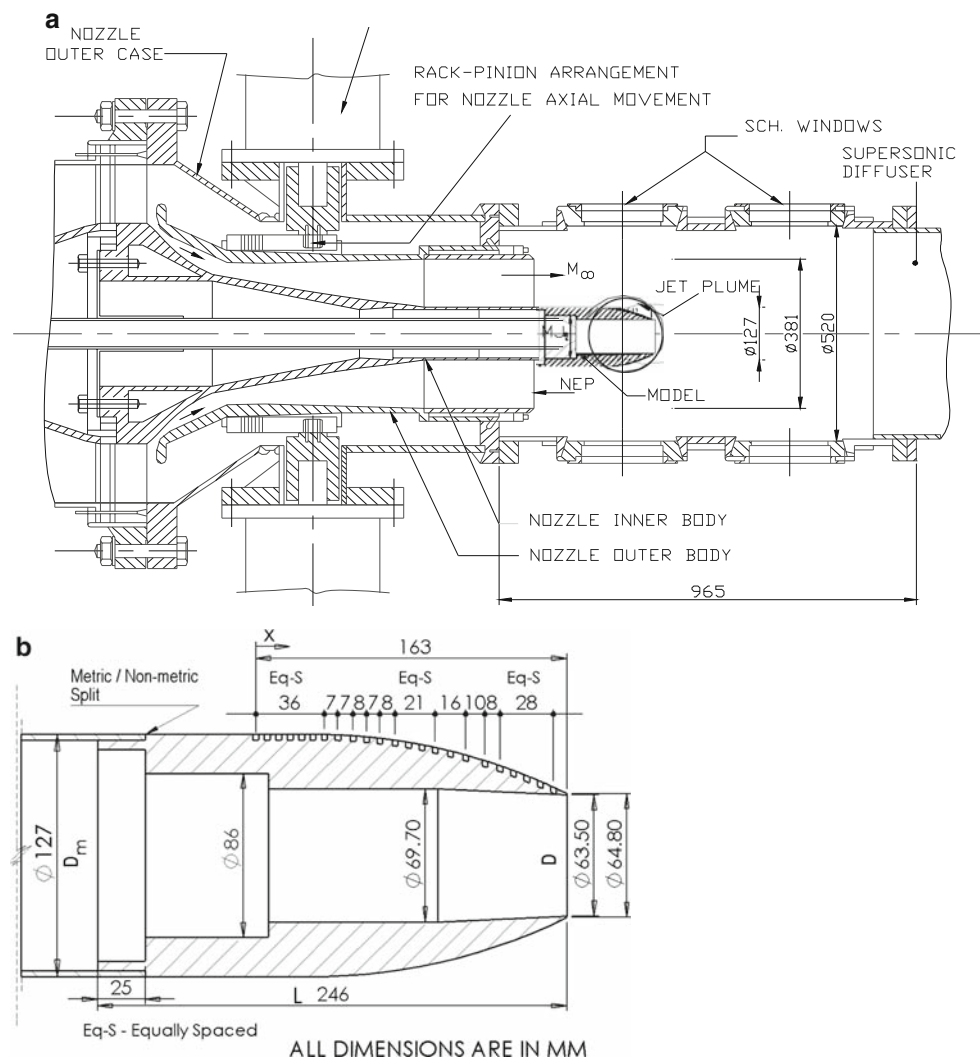
NASA investigations, see Reubush and Runkel 1973) with a boat-tail angle of 12° (Fig. 2b).

The afterbody with its axisymmetric nozzle (sonic) had a length (L) 246 mm and exit diameter (D) 63.5 mm and was mounted on the center body of diameter (D_m) 127 mm. The afterbody had provision to make longitudinal static pressure measurements with the ports distributed over a distance of 163 mm from nozzle exit as shown in Fig. 2b. Pressure measurements were carried out using a 16-port electronic pressure scanner at 500 Hz, with 250 samples taken for each port location. This resulted in an averaging time of 0.5 s. Four scans were carried out during each run.

Spark Schlieren visualization was carried out by using a PALflash Model 501/s spark source with a flash duration of 750 ns. The Schlieren arrangement was a conventional Z-type arrangement with 9-in. (228 mm) mirrors.

Oil flow visualization was carried out by using a mixture of oleic acid, titanium dioxide powder and SAE 60 grade vacuum pump oil in the ratio of 1:5:7. The consistency of the mixture was arrived at after many trials to ensure adequate movement under shear while not moving under the influence of gravity.

3.2 Experimental conditions

The outer flow (around the afterbody nozzle) was set at $M_\infty = 1.34$. The tunnel blowing pressure (P_o) was 21.02 psia (144.9 kPa) and temperature (T_o) was 300 K. As stated earlier, both jet-off and jet-on conditions were studied. The nozzle was physically blocked off for the jet-off condition so as to ensure that there were no flow interactions with the jet cavity. This would enable proper comparison with the jet-on case. For the jet-on case, the jet was run at an underexpanded condition of $P_{oj}/P_\infty \sim 6$, which corresponded to a degree of expansion $P_e/P_\infty = 2.8$. The jet settling chamber (P_{oj}) pressure was 40 psia (275.79 kPa) and temperature was 300 K. Preliminary results of the present measurements can be found in Venkatakrishnan et al. (2007).

3.3 BOS experimental procedure

A structured background to focus on was created by means of a dot pattern mounted on a heavy stand fixed on a concrete block to minimize vibrations at a distance of 1.0 m from tunnel centerline (See Fig. 3).

The background was illuminated to achieve better signal to noise ratio by means of a high-powered continuous halogen lamp at the focus of a Schlieren mirror so as to create parallel beam conditions, thus eliminating the need for methods to re-sort sets of fan beam projections into parallel beam projections (Kak and Slaney 1988).

The imaging was achieved by means of a Nikon D1x camera having a resolution of 5.0 M pixels mounted on a heavy stand, fixed to the ground, 1.6 m away from the tunnel. The choice of camera was dictated by the higher resolution (5.0 M pixels) available as opposed to most scientific grade cameras (usually 2.0 M pixels). Earlier experiments (Venkatakrishnan and Meier 2004) with both camera revealed that number of pixels mattered more than pixel sensitivity for BOS measurements.

BOS measurements were made using the above camera in continuous light with camera exposure fixed at 1/3,200 s—this enabled capturing certain gross unsteadiness often associated with shock–boundary layer interaction and 19 frames of BOS were used to obtain a meaningful mean density field. Since the interest was in documenting the mean density field, a relatively large exposure time of 1/3,200 s was chosen (which would still capture the large scale unsteadiness associated with the flow). Based on our earlier studies (Venkatakrishnan and Meier 2004 and Venkatakrishnan 2005), it was found that about eight fields of BOS data were sufficient to obtain meaningful averages. Hence, 25 BOS images were obtained over five separate blowdowns out of which six had to be discarded due to the slight blurring of the background (as a result of vibration). The effectiveness of the method is proven by examination of Fig. 9 (discussed later). A 300-mm lens was employed for the imaging which resulted in a scaling of 0.09 mm pixel^{-1} (for the nozzle plane). The sensitivity was such that the maximum
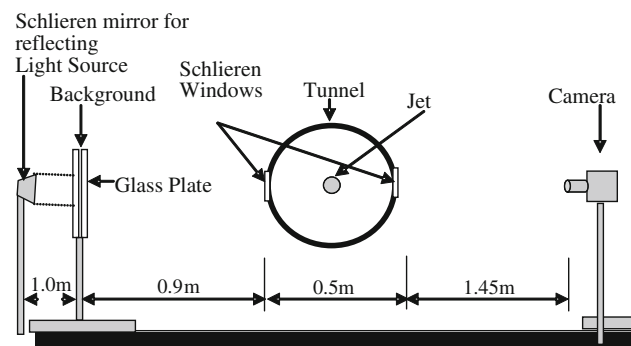
displacement of the background was about 3 pixels. The interrogation window size used was 16×16 pixels resulting in a density field resolution of 1.4×1.4 mm.

The Schlieren windows provided the optical access for the BOS imaging. The optimal location for the background, light source, and camera were arrived at by using the methodology outlined in Venkatakrishnan and Meier (2004) and keeping in mind that increasing sensitivity (displacement of image) meant lower physical resolution as the interrogation size used in the correlation algorithm would have to be correspondingly larger.

The 3D reconstruction of the density field was carried out by means of the filtered back-projection technique described in Venkatakrishnan and Meier (2004) and Venkatakrishnan (2005). Assuming axisymmetry of the flow meant that a single view was the same as an infinite number of views and allowed the full reconstruction of the mean density field.

While it was possible to image the instantaneous density field using a short-duration (<1 μs) light source, the reconstruction would need simultaneous imaging from adequate number of view angles for achieving 3D instantaneous density field. This was not possible in the present case due to the optical access being limited to the Schlieren windows. Hence, only continuous light was used.

Conventional horizontal knife-edge spark Schlieren visualization was also carried out using the same short-duration flash source to enable a qualitative comparison of the BOS results.

4 Repeatability and measurement uncertainty

The model static pressure measurements were made employing a 10-psid ESP scanner frequently calibrated during the test series. The uncertainty estimated, using the method suggested by Kline and McClintock (1953) and taking into account repeatability, was $Cp < \pm002Cp$ (±0.1 psi $- 689.5$ Pa); this corresponds to a $P_s/P_\infty < \pm 0.025$. The variation in tunnel blowing pressure and jet pressure was $\pm1\%$.

5 Results and discussion

Experiments were carried out at a freestream Mach number of 1.34 which was dictated by the consideration that the shock had to be visible in the Schlieren window. The sonic jet was run underexpanded at a jet pressure ratio ($JPR = P_{oj}/P_\infty$) of 6 corresponding to a degree of under-expansion (P_e/P_∞) of 2.8.

Surface static pressure measurements were made simultaneous with the BOS imaging. Density calculated

Fig. 3 Schematic of experimental setup

using the pressure data from the port just upstream of the shock enabled the determination of the integration constant in step (b) described earlier in the section on BOS methodology.

In the following sub-sections, results from the jet-off case are discussed first followed by the jet-on case. Data from oil flow visualization are presented followed by results from the surface pressure measurements, Schlieren visualizations and finally quantitative density fields derived from BOS.

5.1 Results at $M_\infty = 1.34$ and $JPR = 0$ (Jet-off)

5.1.1 Static pressure measurements

Results from the mean surface static pressure measurements are shown in Fig. 4. As may be seen in the figure, the pressure is constant on the cylindrical portion (ahead of the afterbody) and it falls gradually due to the expanding flow on the afterbody; the pressure rises towards the end of the afterbody ($x/L > 0.8$) due to the oblique shock–boundary layer interaction. The limited pressure data shows a significant relief in the adverse pressure gradients following separation of the boundary layer. The Mach number distribution (determined from surface pressure distributions by assuming isentropic relations) show variations as expected; the Mach number increases to a value of about 1.74 from the value of 1.34 on the cylindrical portion and then decelerates across the oblique shock.

5.1.2 Results from oil flow visualization

Figure 5 shows the result of surface flow visualization which reveals separation of the boundary layer upstream of the nozzle exit; a small degree of non-axisymmetry may be
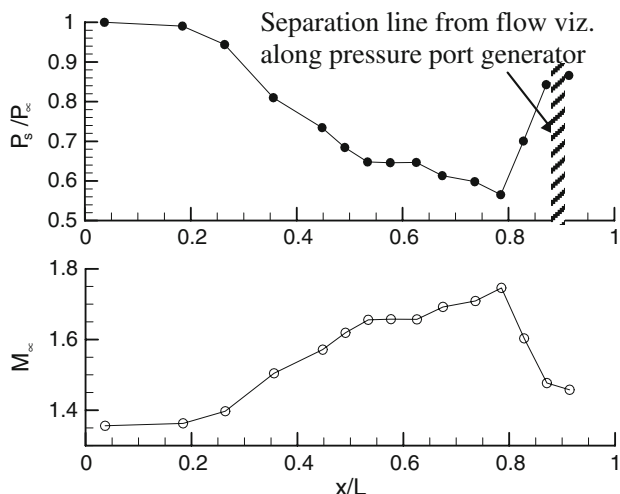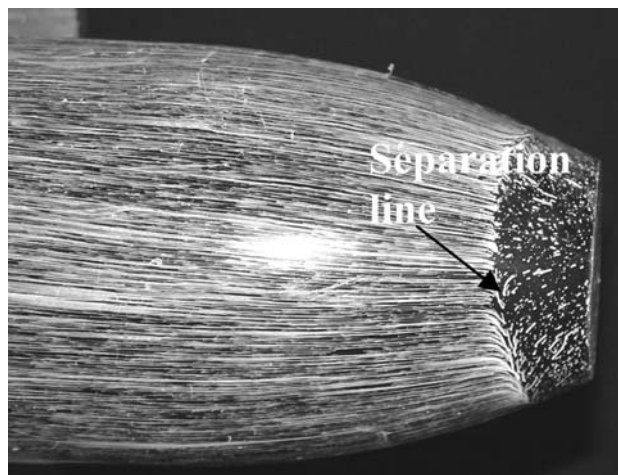

Fig. 5 Typical oil flow patterns on afterbody at $M_\infty = 1.34$ for jet-off condition

observed—separation on the bottom part occurs about 1–2 mm downstream compared to the separation on the top half. The flow separation occurs at about 18–20 mm ($\sim 2.2\delta_o$) upstream ($\sim 0.12L$) of the nozzle exit. This flow separation location is also shown in Fig. 4.

5.1.3 Spark Schlieren visualization

Figure 6a and b show two instantaneous conventional Schlieren images (horizontal knife-edge) of downstream locations of the shock and separation—these frames were selected after examining a set of 25 Schlieren images. The 25 images were taken over five different runs with five images which were captured at 3-s intervals. The spark duration was 750 ns. Close examination of the images show the compression waves coalescing into the shock wave in the inviscid region of the flow. The mild asymmetry seen in the oil flow visualization is seen here too with the shock location on the lower surface relatively closer to the nozzle lip as seen in Fig. 6b. The flow showing the extreme upstream and maximum shock excursion was estimated to be about 14 mm which is about $2\delta_o(0.86L)$. The shock angle measured from the Schlieren images is about 20° which agrees with that (19.25°) calculated using isentropic relations from pressure port data. The dead-air region just downstream of the afterbody is captured in the images. The reattachment/closure of the wake occurs downstream of the base which could not be captured in the measurements due to limited view available in the Schlieren window.

5.1.4 BOS measurements

Figure 7 shows the gradients of the mean line-of-sight integrated density field obtained by correlation of no-flow and flow images averaged over 19 fields each of which was

Fig. 4 Static pressure variation on afterbody at $M_\infty = 1.34$ for jet-off condition
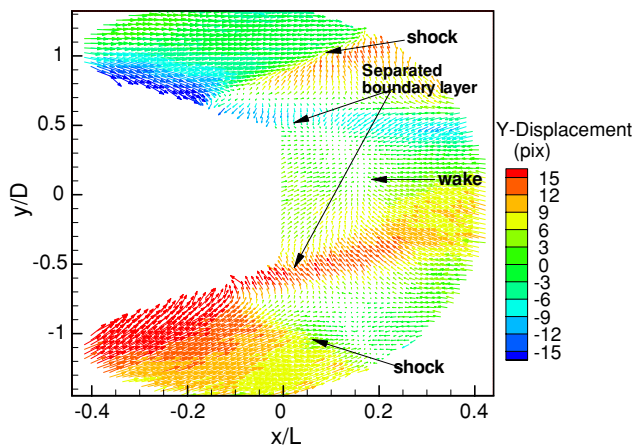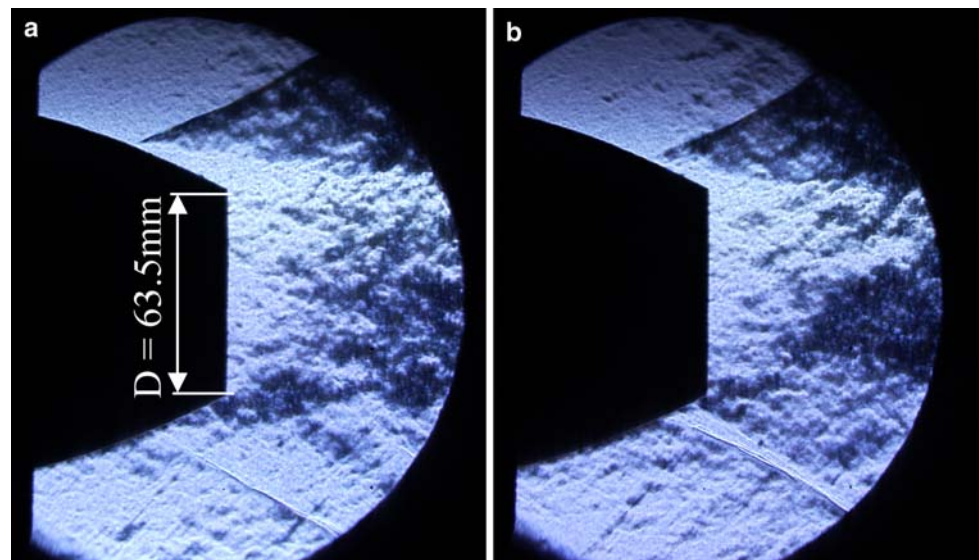
Fig. 7 Averaged vector field of density gradients for jet-off condition
using continuous light source (line-of-sight integrated)

obtained from a realization of the background (with flow),
using an exposure time of 1/3,200 s. As brought out earlier,
this averaging of even long duration exposures is necessitated due to the randomness of the shock excursion. The
vectors point in the direction of lower density and are
color-coded to show the varying magnitude of the vertical
(y) gradients that correspond to a horizontal knife-edge
Schlieren. Alternate vectors are skipped for clarity. This is
equivalent to a time-averaged Schlieren image and shows
the averaged position of the oblique shocks and also the
separated boundary layer. The gradient field shows the
asymmetry noticed earlier in the surface flow visualization.
The reattachment occurs much downstream of the Schlieren window and is not visualized.

The 3D reconstruction of mean density field for the jet-off
case is presented in Fig. 8a. The reconstruction is carried out

by using the 19 images, which are not simultaneous; this hence
yields the mean density field. The volume visualized has been
cutaway to the depth corresponding to nozzle centerline to
show the flow features. In addition, a slice through the nozzle
diameter (xz plane) illustrates the behavior of the flow
downstream of the body and the z-plane slice shows the axisymmetric nature of the flow. The figure reveals the shock
surface, separated boundary layer and the flow behind the
nozzle exit plane. The small non-axisymmetry seen in the
visualization earlier is not seen here due to axisymmetry of
mean flow assumed in reconstruction.

The density is normalized by the freestream density at
$M_\infty = 1.34$ (calculated from the first pressure port data on
the cylindrical portion) Examination of the figures shows
that the area of dead-air region (shown in blue) behind the
base varies between 40 and 50% of the freestream density.

Figure 8b shows the central plane of the mean density
field extracted from the reconstructed density field presented in Fig. 8a. The figure clearly shows the boundary
layer separation occurring around 18 mm (0.11L) upstream
of nozzle exit as was obtained from the surface flow
visualization results (Fig. 5). Figure 9 plots a comparison
of the density calculated from the pressure ports on the
nozzle surface against that obtained from BOS at a vertical
location of about δ_o from the surface. The density has been
calculated using the boundary layer approximation for
attached flow. Beyond the shock location the assumption of
attached flow is no longer valid; hence the calculated
density is shown as a dotted line. The extent of BOS data is
restricted to the region of view seen through the schlieren
window. The agreement is extremely good until the shock
location. The shock is 'smeared' over a larger streamwise
extent in the BOS data due to finite size of the interrogation
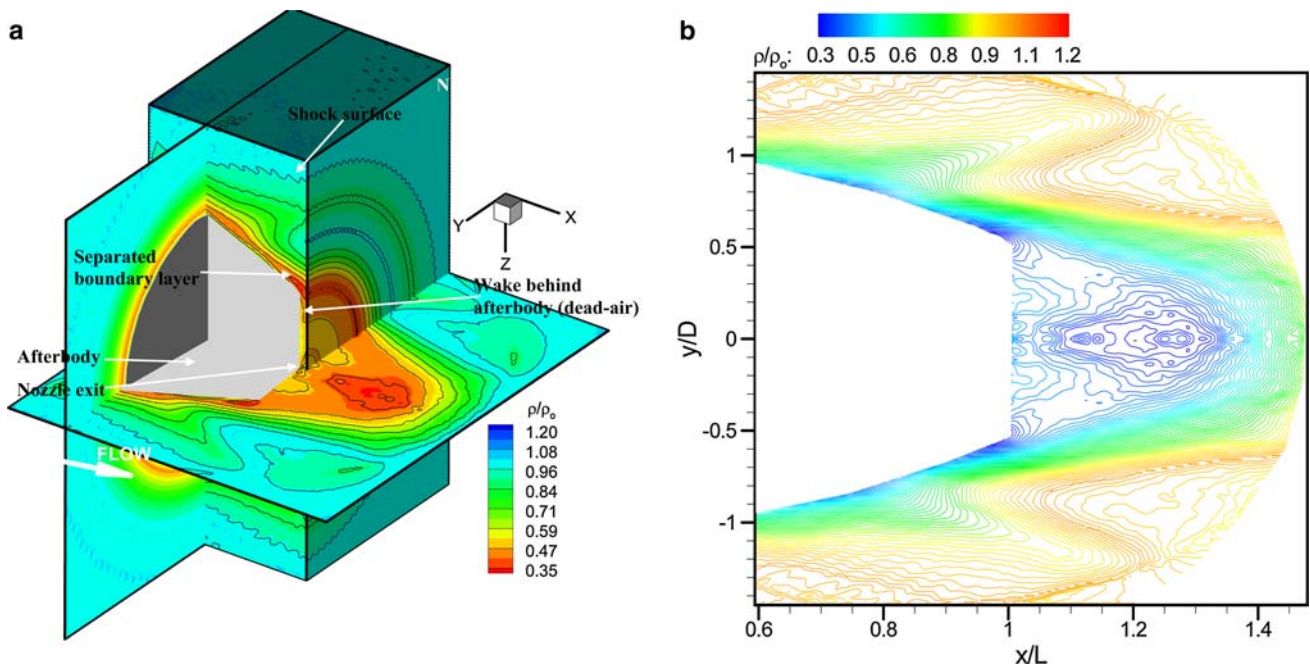area and due to the effect of averaging over 19 fields.

Fig. 8 a 3D reconstruction of mean density field for the jet-off case. **b** Central plane showing mean density contours at $M_\infty = 1.34$ for jet-off condition
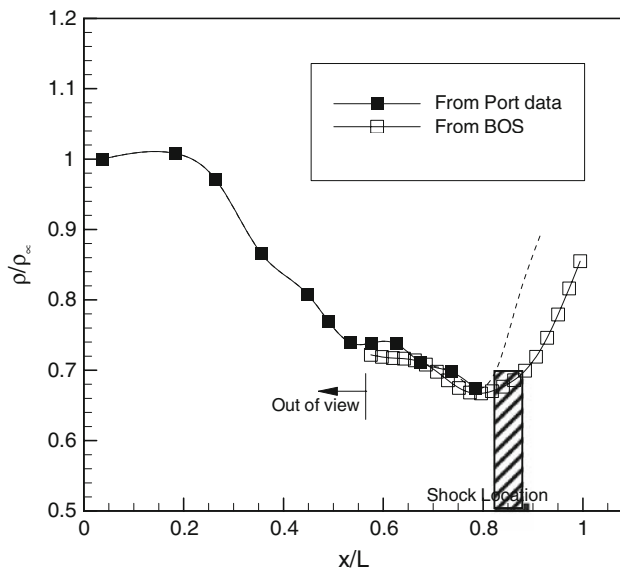

Fig. 9 Comparison of normalized density values obtained from BOS against pressure port data

Fig. 10 Static pressure variation on afterbody at $M\infty = 1.34$ for jet-on condition

The rise in density across the shock ($\rho_2/\rho_1 = 1.78$) matches that calculated from using oblique shock relations ($\rho_2/\rho_1 = 1.73$), thus validating the BOS procedure.

5.2 Results at $M_\infty = 1.34$ and $JPR = 6$ (Jet-on)

5.2.1 Static pressure measurements

Mean surface static pressures for the jet-on case shown in Fig. 10 suggest an upstream shift of the oblique shock;
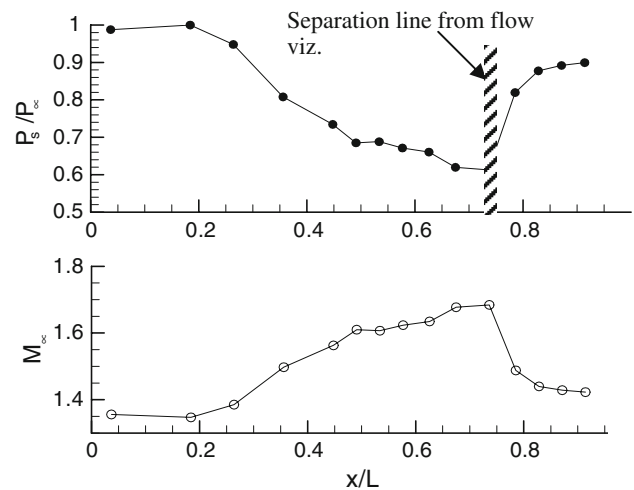
separation occurs further upstream—$0.75x/L$—(compared to no-jet case); increased bubble size is indicated by the larger zone of plateau pressure. This is due to the positive pressure field imposed by the underexpanded jet plume on the afterbody boundary layer. The figure also shows the corresponding Mach number plotted as a function of normalized distance from the first pressure port. The data show the oncoming freestream flow at $M_\infty = 1.34$ which accelerates to a value of $M = 1.68$, followed by a shock which decelerates the flow to $M = 1.4$; thereafter, the flow is separated till the nozzle exit.
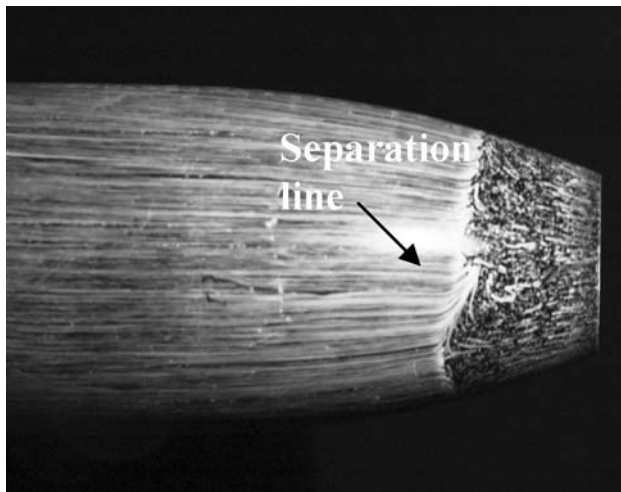
Fig. 11 Typical oil flow patterns on afterbody at $M_\infty = 1.34$ for jet-on condition

5.2.2 Results from oil flow visualization

Figure 11 shows the results of oil flow visualization on the afterbody at freestream Mach number of 1.34 for the jet-on condition. The slight asymmetry of the separation line which was observed in the jet-off case has reduced significantly due to the fact that the axisymmetric jet plume plays the dominant role in determining the flow topology on the afterbody. In the presence of the jet, the separation line is found to be pushed upstream and occurs at about 36 mm ($4.8\delta_\mathrm{o} - 0.22L$) upstream of the nozzle exit.

5.2.3 Spark Schlieren visualization

Figure 12a and b show instantaneous Schlieren images at two instances for the $JPR = 6$ case. The images were chosen
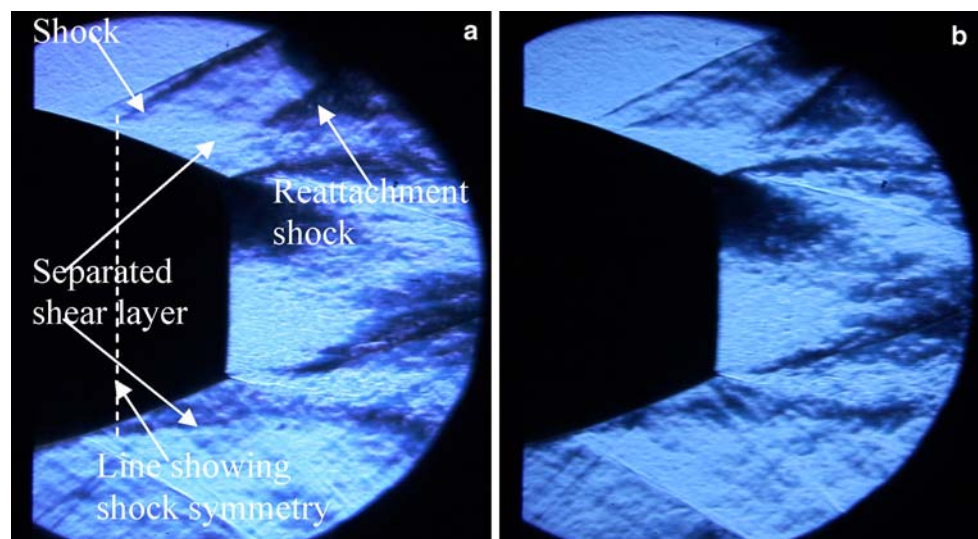
to show the extreme locations of the shock excursion. It may be seen that the oblique shock and the associated separation are pushed further upstream consistent with the measured pressure distribution. The first image shows the shock occurring at a distance of 40 mm upstream ($0.245L$) of nozzle exit. The distance of the shock excursion is about 8 mm ($0.05L$) which is significantly lower than that for the jet-off case (14 mm $- 0.86L$). The mean separation point obtained from this measurement is about 36 mm ($0.22L$) which agrees well with that from the oil flow visualization data. The flow separates slightly upstream of the shock and the point of reattachment is on the jet shear layer at a distance between 18 and 20 mm ($\sim 0.12L$) downstream of nozzle exit. The reattachment shock is seen at this location.

5.2.4 BOS measurements

Figure 13 shows the vector map of line-of-sight integrated density gradients obtained from the average of 19 long exposures (1/3,200 s) using the continuous light source. The averaging was done as the shock excursions were random—as in the jet-off case. It is immediately seen that the flow field is significantly more axisymmetric in the jet-on case (as also revealed by surface and Schlieren flow visualization) since the jet dynamics play a dominant role in the upstream development including the point of separation of the boundary layer. The density gradient field captures the various flow features of shock, separated shear layer, reattachment on jet plume, etc.

Due to the high underexpansion (*JPR* of 6; $P_e/P_\mathrm{oj} \sim 0.5$), the exit structure of the jet is characterized by an expansion fan with higher density values towards the jet centerline and lower towards the periphery, which is clearly visible in the figure.
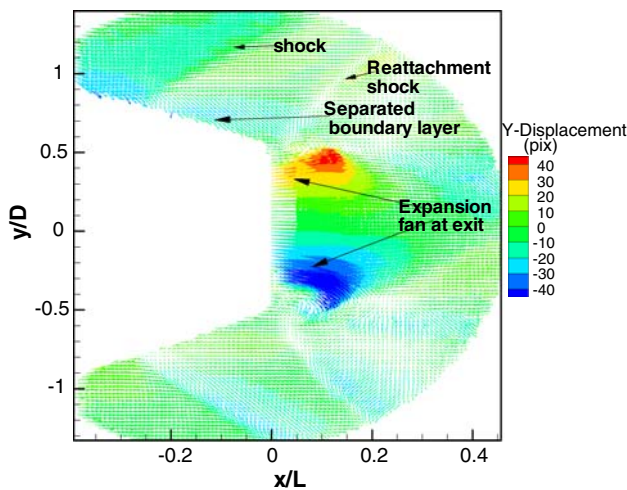
Fig. 12 a Instantaneous Schlieren image at $M_\infty = 1.34$ for jet-on condition showing maximum upstream location of shock. **b** Instantaneous Schlieren image at $M_\infty = 1.34$ for jet-on condition showing maximum downstream location of shock

Fig. 13 Averaged vector field of density gradients at $M_\infty = 1.34$ for jet-on condition

Figure 14a presents the 3D reconstruction of the afterbody nozzle with the jet flow. The flow features including the shock cells of the underexpanded jet are clearly seen.

Figure 14b presents the mean density field in the central plane for the jet-on condition. The rise in density across the shock ($\rho_2/\rho_1 = 1.56$) matches that calculated using shock relations ($\rho_2/\rho_1 = 1.6$). The flow topology is dominated by the pressure field of the underexpanded jet. For the present degree of underexpansion, the jet exit density normalized by the freestream value (ρ_{jet}/ρ_∞) is 1.18 from the BOS data and 1.2 from isentropic relations. The separated boundary layer reattaches on the jet shear layer resulting in a reattachment shock accompanied by a density rise as is seen in Fig. 14b at $x = 30$ mm ($x/L = 1.18$) downstream of exit.

Figure 15 plots the variation of the normalized mean density in the vertical direction at different x/L locations. The y-axis is aligned at $\rho/\rho_\infty = 1$ so as to easily discern density changes relative to the freestream. The plot presents data for both jet-off and jet-on cases. At $x/L = 0.7$, for jet-off case (shock location $x/L \sim 0.85$), the flow has not yet separated and the effect of the adiabatic wall is manifested in a lower density near the surface which increases to the freestream value. At this location, for the jet-on case (shock location $x/L \sim 0.75$), the upstream effect of the shock on the boundary layer which is about to separate is seen. This is seen from the increase in the density near the surface. The effect of the shock (for jet-on case) at $x/L \sim 0.75$ is reflected in the higher density compared to the jet-off case. The density returns to freestream value beyond $y/D = 1.2$ due to the larger distance from the (inclined) shock. At $x/L = 0.9$, the boundary layer has separated for both cases, leading to a low-density region near the surface created by the low-pressure wake region for the jet-off case and the expansion fan of the underexpanded jet in the jet-on case. The different degrees of boundary layer separation account for the differences in density for the two cases at $y/D = 0.9$. The next location for comparison is at $x/L = 1.05$, just downstream of nozzle exit. At this location, data are available from model centerline; the decrease in density due to the wake in the base flow region for the jet-off case is seen. For the jet-on case,
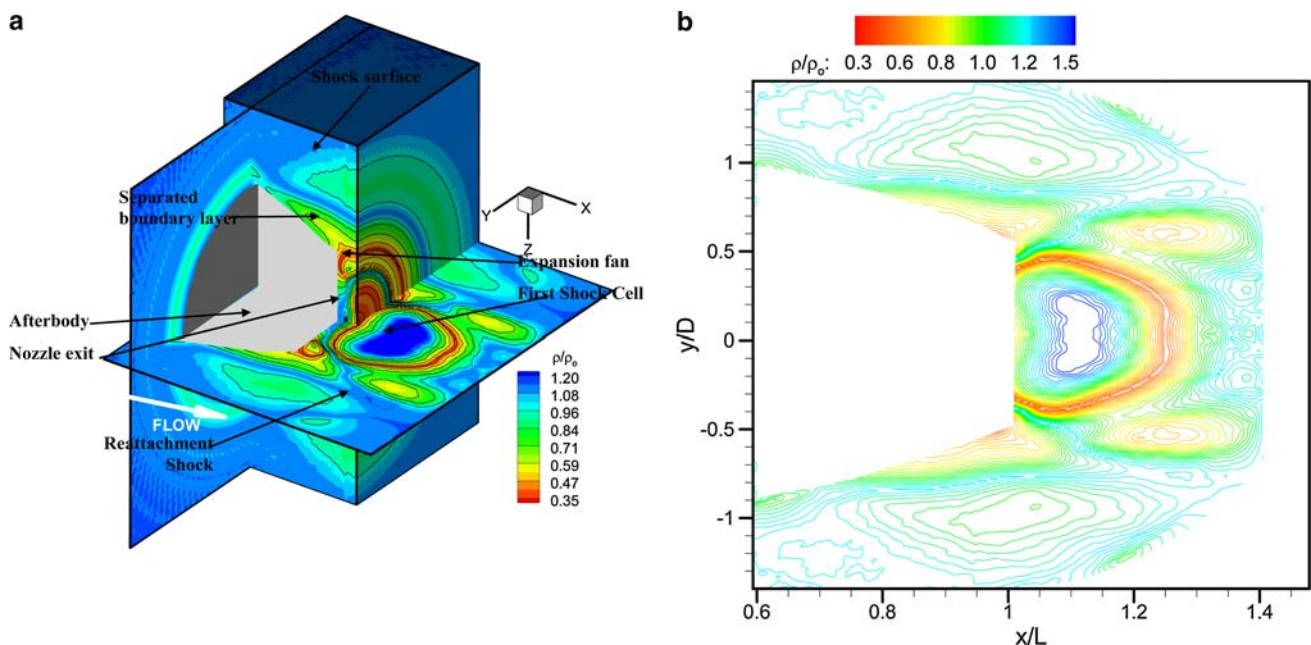

Fig. 14 a 3D reconstruction for jet-on condition. **b** Central plane showing mean density contours obtained using BOS technique for jet-on condition
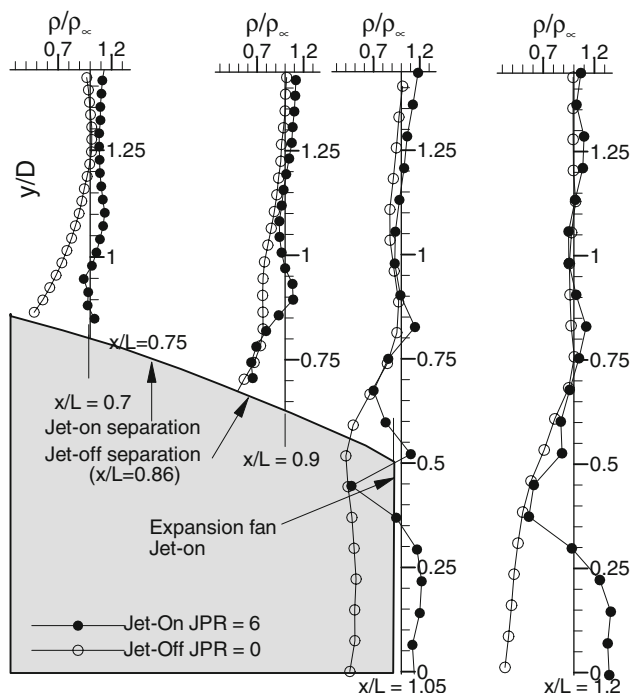
Fig. 15 Mean density variation in vertical direction for different axial locations for both cases

the jet density at centerline matches the isentropic calculation of $\rho_{jet}/\rho_\infty = 1.2$. Away from the centerline, the lowered density due to the expansion fan at the jet corners is observed. At the locations of $y/D = 0.8$ and 1.25, there is a difference of about 0.2 in the normalized density. While at $y/D = 0.8$ this is because of the deflection of the separated shear layer due to the presence of the jet, at $y/D = 1.25$ it is due to the effect of the reattachment shock at that point. At the final station of $x/L = 1.2$, the wake of the base flow in the jet-off case is still not closed, leading to density lower than freestream. For the jet-on case the higher density due to the underexpanded jet is seen below $y/D = 0.3$ followed by a sudden decrease through the expansion fan at the nozzle edges.
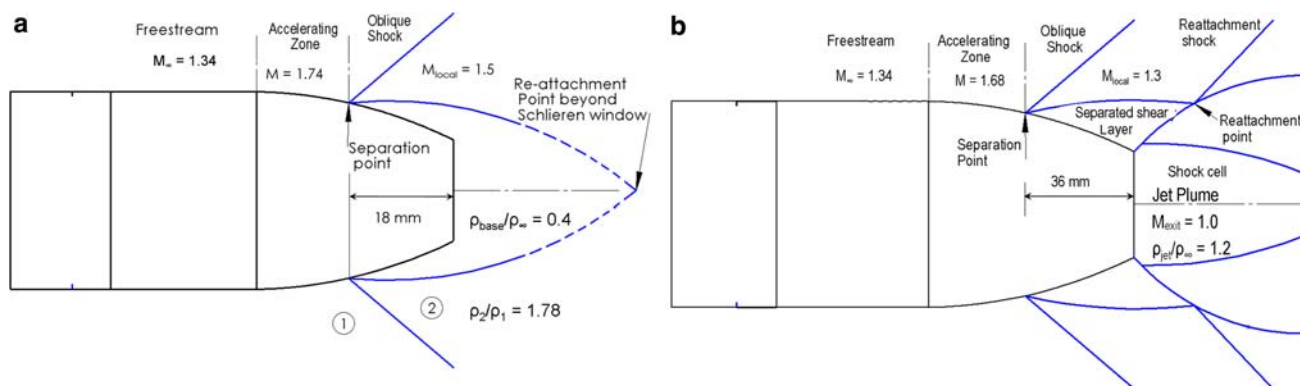
The flow topology for both cases is drawn as shown in Fig. 16. The broad features of the flow include an isentropic expansion of the freestream Mach number (1.34) over the initial part of the afterbody reaching a value of 1.74 for jet-off and 1.68 for the jet-on conditions, respectively. This difference arises from the positive pressure field produced by the underexpanded jet which pushes the separation point relatively upstream. This results in a shorter zone of acceleration for the flow.

Immediately downstream of the shock, the Mach numbers are correspondingly different reaching 1.5 and 1.4 for jet-off and jet-on, respectively. The flow separates at about 18 mm for the jet-off and 36 mm for the jet-on conditions, i.e., at x/L of 0.12 and 0.22, respectively. The reattachment or wake closure occurs much farther downstream for the jet-off case compared to the jet-on case where reattachment is on to the jet shear layer. This results in a reattachment shock. The dotted lines indicate that the flow is beyond the view of the Schlieren window.

6 Conclusion

The BOS technique has been successfully applied to map the mean density field of an oblique shock-separated turbulent flow on an axisymmetric afterbody. The measurements were made at a freestream Mach number of 1.34 and both mean density fields were acquired using BOS technique both without and with a central sonic jet. Data from spark Schlieren showed significant excursion of the oblique shock on the afterbody which was about 14 and 8 mm for the jet-off and jet-on case, respectively.

The density field is relatively more axisymmetric for the jet-on case as compared to the jet-off case, since the jet dynamics play a dominant role in the upstream development including the point of separation of the boundary layer. The data obtained also show the mean density in the base region (jet-off case) to be about 50% of the freestream

Fig. 16 Flow topology for jet-off and jet-on conditions

density and match the isentropic values for the underexpanded jet at the exit. The data extracted from the mean density field obtained through BOS have been compared for the jet-off and jet-on cases. The comparisons clearly show the differences in the density field for the two cases due to the different separation locations and the re-attachment shock in the second case. Based on the measurements a mean flow topology has been drawn for both the jet-off and jet-on cases.

The data present a clear picture of the density field in this complex flow where other density measurement techniques are extremely difficult and hence would be extremely useful for understanding and CFD code validation.

References

Bergman D (1971) Effects of engine exhaust flow on boat-tail drag. J Aircr 8(6):434–439

Boswell BA, Dutton JC (2001) Flow visualizations and measurements of a three-dimensional supersonic separated flow. AIAA Stud J 39(1):113–121

Dalziel SB, Hughes GO, Sutherland BR (2000) Whole field density measurements by synthetic Schlieren. Exp Fluids 28:322–335

Decamp S, Kozack C, Sutherland BR (2008) Three-dimensional schlieren measurements using inverse tomography. Exp Fluids 44(5):747–758

Delery J, Sirieix M (1979) Base flows behind missiles. ONERA TP 1979-14E

Depres D, Reijasse P, Dussauge JP (2004) Analysis of unsteadiness in afterbody transonic flows. AIAA Stud J 42(12):2541–2550

Goldhahn E, Seume J (2007) The background oriented schlieren technique: sensitivity, accuracy, resolution and application to a three-dimensional density field. Exp Fluids 43(2):241–249

Kak AC, Slaney M (1988) Principles of computerized tomographic imaging. IEEE, New York

Kline SJ, McClintock FA (1953) Describing uncertainties in single-sample experiments. Mech Eng 75:3–8

Mathur NB, Viswanath PR (2004) Studies on square base afterbodies. J Aircr 41(4):811–820

Mathur NB, Yajnik KS (1990) Underexpanded jet-freestream interactions on an axisymmetric afterbody configuration. AIAA Stud J 28(1):47–50

Meier GEA (2002) Computerized background oriented Schlieren. Exp Fluids 33(1):181–187

Midgal D, Miller EH, Schnell UC (1969) An experimental evaluation of exhaust nozzle/airframe interference, AIAA 1969-430. Fifth Joint Specialist Conference, USAF Academy, Colorado Springs, CO

Onu K, Flynn MR, Sutherland BR (2003) Schlieren measurement of axisymmetric wave amplitudes. Exp Fluids 35(1):24–31

Raffel M, Richard H, Meier GEA (2000) On the applicability of background oriented optical tomography for large scale aerodynamic investigations. Exp Fluids 28:477–481

Reijasse P, Bernard C, Delery J (1997) Flow confluence past a jet-on axisymmetric afterbody. J Spacecr Rockets 34(5):593–601

Reubush DE, Runkel JF (1973) Effect of fineness ratio on boat-tail drag of circular-arc afterbodies having closure ratios of 0.50 with jet exhaust at Mach numbers up to 1.30. NASA TN D-7192

Sutherland BR, Linden PF (2002) Internal wave excitation by a vertically oscillating elliptical cylinder, phys. Fluids 14:721–731

Sutherland BR, Dalziel SB, Hughes GO, Linden PF (1999) Visualization and measurement of internal gravity waves by 'Synthetic Schlieren'. Part I. Vertically oscillating cylinder. J Fluid Mech 390:93–126

Venkatakrishnan L (2005) Density measurements in an axisymmetric underexpanded jet using background oriented Schlieren technique. AIAA Stud J 43(7):1574–1579

Venkatakrishnan L, Meier GEA (2004) Density measurements using background oriented Schlieren technique. Exp Fluids 37(2):237–247

Venkatakrishnan L, Suriyanarayanan P, Mathur NB (2007) BOS density measurements in afterbody flows with shock and jet effects, Paper AIAA 2007-4223, 37th AIAA fluid dynamics conference and exhibit